Heterogenisation of a Carbonylation Catalyst on Dispersible Microporous Polymer Nanoparticles

Samuel A. Ivko,[a,b] Alex M. James,[a,c] Matthew J. Derry,[d] Robert Dawson[a] and Anthony Haynes[a]*

[a] Department of Chemistry, University of Sheffield, Sheffield, S3 7HF, UK

Email: a.haynes@sheffield.ac.uk

[b] Current address: School of Chemistry, University of Birmingham, Birmingham, B15 2TT, UK

[c] Current address: Materials Innovation Factory, University of Liverpool, Liverpool, L7 3NY, UK

[d] Aston Institute of Materials Research, Aston University, Birmingham, B4 7ET, UK

Supporting Information

S1. Materials and synthetic methods

Dry CH_2Cl_2, $CHCl_3$, toluene and *n*-hexane were obtained from a Grubbs solvent purification system in which the solvents were degassed prior to being passed through activated alumina and a supported copper catalyst to remove protic contaminants and trace oxygen respectively.[1] These solvents were stored under N_2 and used within 24 h of collection from the dry solvent system. Other solvents were purchased from either Fisher Scientific or Sigma-Aldrich (HPLC grade unless otherwise stated) and were used without further purification. Monomers divinylbenzene (DVB, technical grade 80%, Sigma Aldrich) and 4-vinyl pyridine (4VP, 95%, Sigma Aldrich) were passed through alumina to remove the inhibitor prior to polymerisation. Other reagents were purchased from either Fisher Scientific or Sigma-Aldrich and used without further purification. Rhodium trichloride hydrate ($RhCl_3.xH_2O$) was purchased from Precious Metals Online and rhodium precursors $[Rh(CO)_2Cl]_2$ and $[Rh(CO)_2I]_2$ were synthesised according to literature procedures.[2, 3] Standard Schlenk techniques and glassware were used for preparative reactions.

S2. Instrumentation

Infra-red spectra of polymeric materials and supported catalyst were collected using a Perkin-Elmer 100 FTIR spectrometer. Samples were prepared by grinding with a 20× excess of pure KBr pre-dried overnight in a vacuum oven at 80 °C. The sample was pelletised at high pressure (10 tons) and analysed as a thin transparent disc.

Nitrogen gas sorption isotherms were collected at 77 K using approximately 100 mg of sample on an ASAP 2020 Micromeritics volumetric adsorption analyser. Prior to analysis all samples except **3** were degassed for at least 16 h at 120 °C under a vacuum of at least 10^{-5} bar. **3** was degassed under the same vacuum level but without heating to avoid any decomposition of the supported Rh complex. BET surface areas were calculated over a relative pressure range

of 0.01 – 0.15 p/p_0. Pore size distributions and pore volumes were calculated from the adsorption isotherms and modelled using the nonlocal density functional theory model (NL-DFT) for N_2 on carbon slit pores found within the micromeritics ASAP software.

Solid-state NMR samples were packed into 4 mm zirconia rotors and transferred to a Bruker Avance III HD spectrometer. 1D ^{1}H-^{13}C cross-polarisation magic angle spinning (CP/MAS) NMR experiments were measured at 125.76 MHz (500.13 MHz 1H) at a MAS rate of 10.0 kHz. The ^{1}H $\pi/2$ pulse was 3.4 μs, and two-pulse phase modulation (TPPM) decoupling was used during the acquisition. The Hartmann-Hahn condition was set using hexamethylbenzene. The spectra were measured using a contact time of 2.0 ms. The relaxation delay, D_1, for each sample was individually determined from the proton T_1 measurement ($D_1 = 5 \times T_1$). Scans were collected until a sufficient signal to noise ratio was obtained, typically greater than 1094 scans. The values of the chemical shifts are referred to that of TMS.

Carbon, hydrogen, nitrogen and sulphur elemental analysis was performed by combustion of an amount of sample in a stream of pure oxygen. The sample was placed in a tin capsule and introduced into the combustion tube of the Elementar Vario MICRO Cube CHN/S analyser via a stream of helium. Combustion products were analysed through after being passed through a copper tube to remove excess oxygen and reduce any NO_x to N_2. Gases were separated using a Thermal Programmed Desorption column and detected using a Thermal Conductivity Detector.

Iodide analysis was performed using the Schöninger flask combustion method in which an amount of sample is combusted in an oxygen-enriched environment, the resultant gases are absorbed and a titration is conducted to determine the iodide concentration.

Dynamic light scattering (DLS) measurements of the polymer solutions were carried out using a Malvern Zetasizer nanoZS instrument *via* the Stokes-Einstein equation which assumes monodisperse, non-interacting spheres.

Transmission electron microscopy (TEM) studies were conducted using a Philips CM 100 instrument operating at 100 kV and equipped with a Gatan 1 k CCD camera. A diluted solution of the polymer material (0.10% w/w) was placed on carbon-coated copper grids, allowed to dry and then exposed to ruthenium(VIII) oxide vapor for 7 min at 20 °C prior to analysis. The ruthenium(VIII) oxide was prepared as follows: Ruthenium(IV) oxide (0.30 g) was added to water (50 g) to form a black slurry; addition of sodium periodate (2.0 g) with stirring produced a yellow solution of ruthenium(VIII) oxide within 1 min.[4]

SAXS patterns were recorded at a synchrotron source (Diamond Light Source, station I22, Didcot, UK; Experiment ID SM23501) using monochromatic X-ray radiation (X-ray wavelength $\lambda = 0.999$ Å, with scattering vector q ranging from 0.0027 to 0.25 Å^{-1}, where $q = 4\pi \sin\theta/\lambda$ and θ is one-half of the scattering angle) and a 2D Pilatus 2M pixel detector (Dectris, Switzerland). Scattering data were reduced and normalised, with glassy carbon being used for the absolute intensity calibration utilising standard routines available at the beamline[5] and further analysed (background subtraction and data modelling) using Irena SAS macros for Igor Pro.[6]

S3. Elemental and ICP-MS analysis data

Elemental analysis data for **1** (Table S1) demonstrate that both DVB and 4VP monomers and the RAFT agent are incorporated into the polymeric material. The nitrogen content is significantly lower than that calculated on the basis of the 1:1 ratio of DVB and 4VP monomers used in the polymerisation reaction. The N content is consistent with an approximate composition for **1** of $PEG_{113}DVB_{300}4VP_{60}$ (i.e. 5:1 DVB:4VP ratio). The iodide content of post-synthetically modified polymer **2** is consistent with quaternisation of ~80% of the pyridine sites in **1**. ICP-MS analysis of **3** indicates a Rh content of 4.5% by mass. Incorporation of a $[Rh(CO)_2I_2]^-$ for each methyl pyridinium site in **2** is calculated to give a Rh content of ~6.9%. Complete incorporation of all Rh added in the synthesis of **3** would give a Rh content of ~6.1%.

Table S1. Elemental analysis data for material **1**, post-synthetically modified polymer **2** and supported Rh catalyst **3**, along with calculated values for different compositions of polymer.

	%C	%H	%N	%S	%I	%Rh
Observed for **1**	87.1	7.7	1.7	0.6		
Calc. for $PEG_{113}DVB_{300}4VP_{300}$	84.5	7.41	5.53	0.13		
Calc. for $PEG_{113}DVB_{300}4VP_{60}$	86.8	7.76	1.66	0.19		
Observed for **2**	76.9	6.9	1.7	0.7	10.5	
Calc. for $PEG_{113}DVB_{300}(4VPMe^+I^-)_{60}$ (full quaternisation)	75.5	6.95	1.42	0.16	12.9	
Calc. for $PEG_{113}DVB_{300}4VP_{12}(4VPMe^+I^-)_{48}$ (80% quaternisation)	77.5	7.09	1.46	0.17	10.6	
Observed for **3**	59.0	5.1	1.9		22.0	4.5*
Calc. for $PEG_{113}DVB_{300}4VP_{12}(4VPMe^+[Rh(CO)_2I_2]^-)_{48}$	64.2	5.73	1.18	0.14	17.1	6.93

*Rh content of **3** determined by ICP-MS

S4. Volumetric gas sorption data

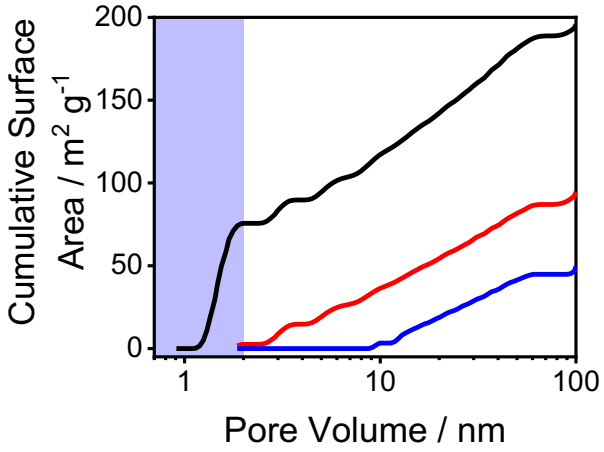

Figure S1. Cumulative surface area *vs*. pore volume for **1** (black), **2** (red) and **3** (blue).

S5. Dispersibility

A sample of **1** was suspended in CH_2Cl_2 and UV-vis spectra of the dispersion were recorded over 72 h (Figure S). Over 80% of **1** remains in suspension after 72 h. Note: in contrast, the insoluble analogue to **1** (synthesised via simple radical polymerisation between 1,4-divinylbenzene and 4-vinylpyridine) could not be suspended for a single UV-vis spectrum to be recorded.

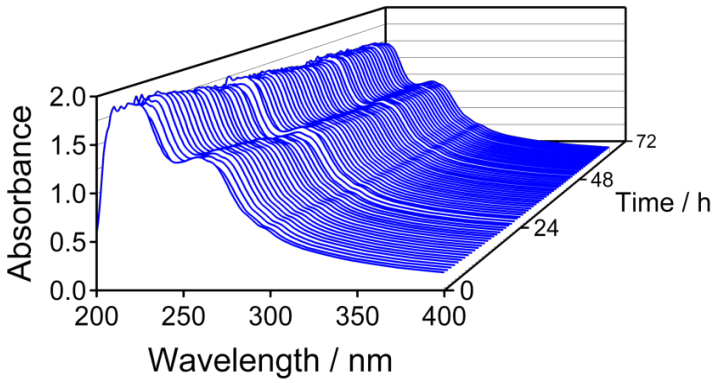

Figure S2. Series of UV-vis spectra of a suspension of **1** in CH_2Cl_2 over 72 h.

S6. Dynamic light scattering (DLS) data

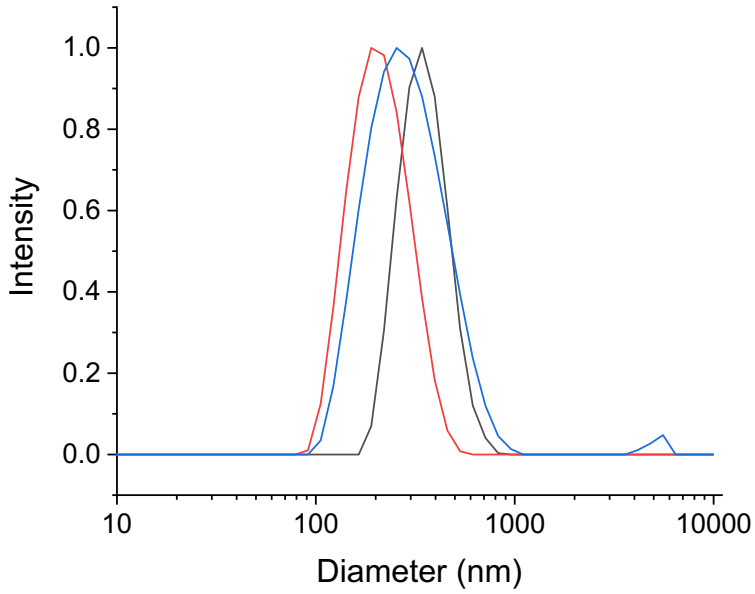

Figure S3. Normalised dynamic light scattering (DLS) particle size distributions of samples **1** (black), **2** (red) and **3** (blue).

S7. Particle morphology

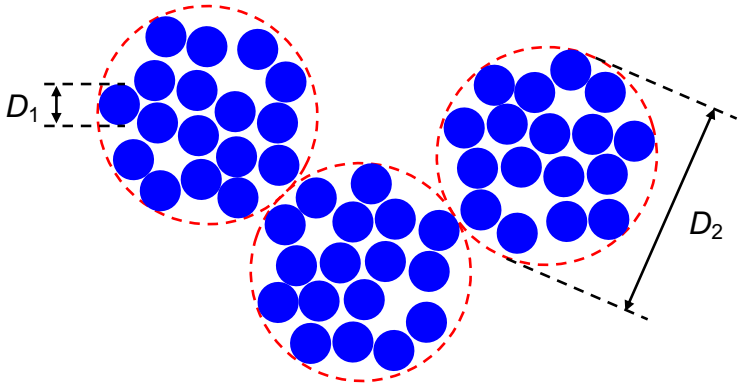

Figure S4. Schematic of particle aggregate morphology.

S8. Kinetic data for reaction of MeI with 3

Table S2. Pseudo first-order rate constants derived from single and double exponential decay fits and their R^2 values for reaction of **3** with MeI in CH_2Cl_2 (25 °C).

[MeI] / mol dm^{-3}	$10^4 \times k_{obs}$ / s^{-1}	R^2	$10^4 \times k_{obs}^1$ / s^{-1}	$10^4 \times k_{obs}^2$ / s^{-1}	R^2
1.0	4.44	0.9791	11.30	2.06	0.9997
2.1	6.25	0.9822	13.34	3.44	0.9998
4.2	10.01	0.9890	17.46	5.15	0.9997
6.2	13.00	0.9862	29.02	5.05	1.0000
8.3	16.52	0.9953	28.88	6.09	1.0000

Fits to a double exponential decay used equation S1 to give values of k_{obs}^1 and k_{obs}^2.

$$A_t = A_\infty + A_1 e^{-k_{obs}{}^1 \times t} + A_2 e^{-k_{obs}{}^2 \times t} \qquad \text{(S1)}$$

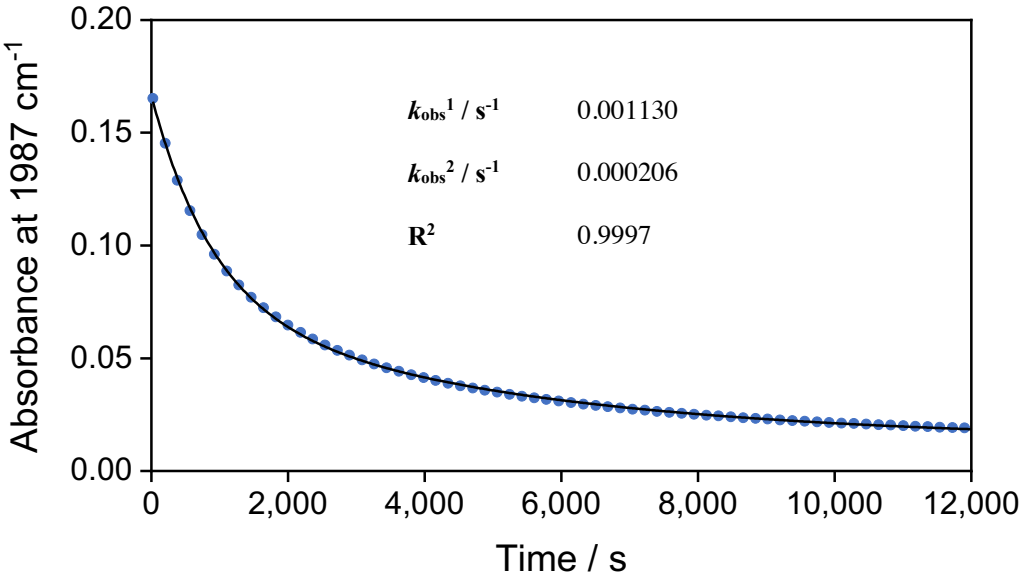

Figure S5. Plot of IR absorbance *vs*. time for band at 1987 cm^{-1} during reaction of **3** with MeI (1.0 M) in CH_2Cl_2 (25 °C). The data are fitted by equation S1.

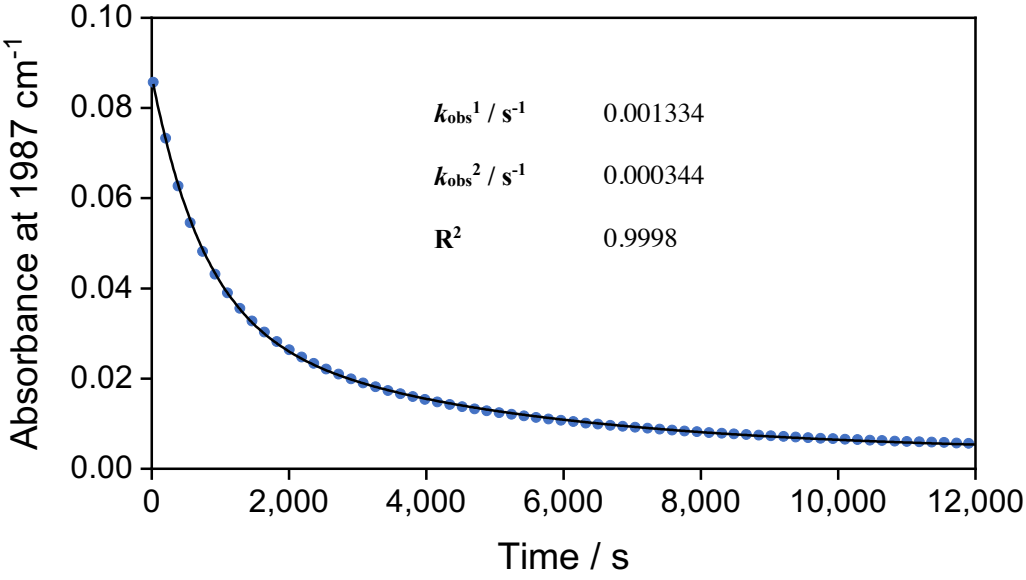

Figure S6. Plot of IR absorbance *vs*. time for band at 1987 cm^{-1} during reaction of **3** with MeI (2.1 M) in CH_2Cl_2 (25 °C). The data are fitted by equation S1.

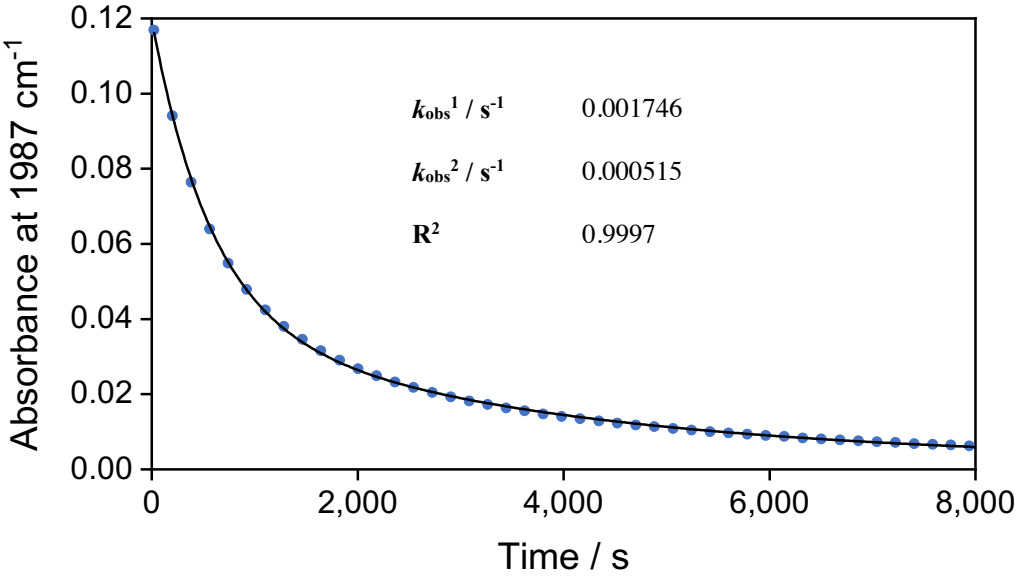

Figure S7. Plot of IR absorbance *vs*. time for band at 1987 cm^{-1} during reaction of **3** with MeI (4.2 M) in CH_2Cl_2 (25 °C). The data are fitted by equation S1.

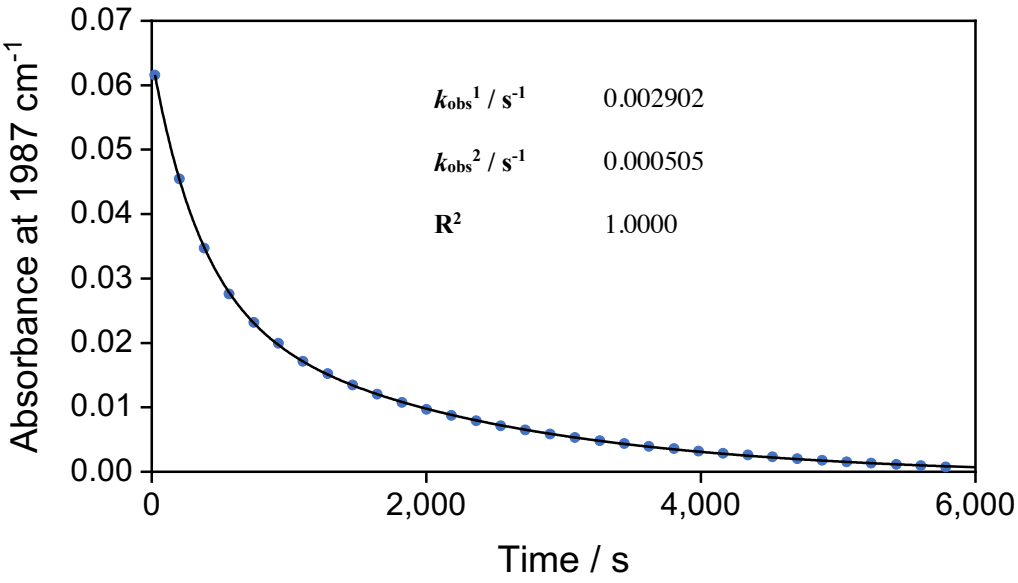

Figure S8. Plot of IR absorbance *vs*. time for band at 1987 cm^{-1} during reaction of **3** with MeI (6.2 M) in CH_2Cl_2 (25 °C). The data are fitted by equation S1.

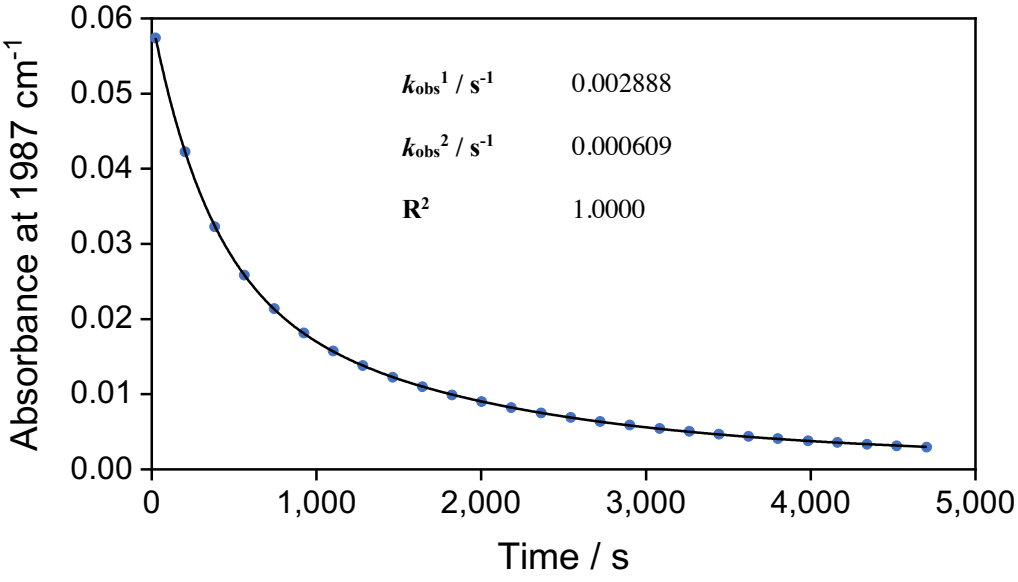

Figure S9. Plot of IR absorbance *vs*. time for band at 1987 cm^{-1} during reaction of **3** with MeI (8.3 M) in CH_2Cl_2 (25 °C). The data are fitted by equation S1.

Table S3. Variable temperature kinetic data and activation parameters for reaction of **3** with MeI (4 M) in CH_2Cl_2. k_{obs}^1 and k_{obs}^2 were determined by fitting absorbance *vs*. time data with the double exponential decay equation S1, as above. Activation parameters are derived from the slopes and intercepts of the Eyring plots in Figure S9.

T / °C	$10^4 \times k_{obs}^1$ / s^{-1}	$10^4 \times k_{obs}^2$ / s^{-1}
7	3.56	0.472
15	8.22	1.08
25	20.0	3.73
37	19.5	4.23
$\Delta H^{\ddagger}$/kJ mol^{-1}	38(±13)	–183(±45)
$\Delta S^{\ddagger}$/J K^{-1} mol^{-1}	51(±14)	–153(±47)

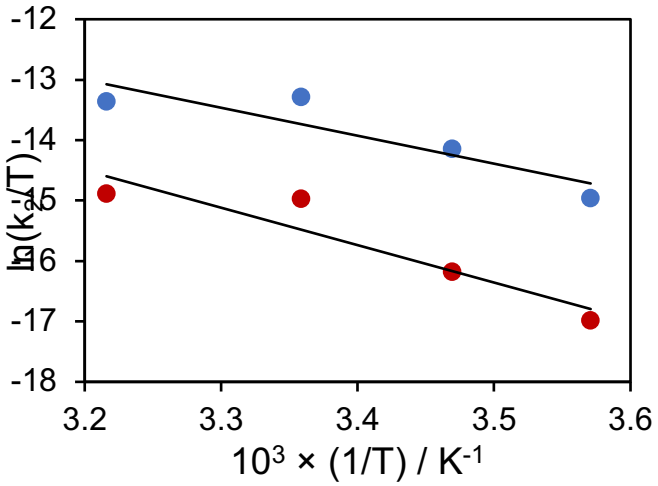

Figure S10. Eyring plots of kinetic data for reaction of **3** with MeI (4 M) in CH_2Cl_2. k_2 values are derived from k_{obs} in Table S3 assuming 2nd order behaviour ($k_2 = k_{obs}$/4 M)

S9. Catalytic carbonylation reactions

Determination of TOF values

For each experiment, the rate of formation of methyl acetate was determined from the slope of a plot of absorbance vs. time for ν(C=O) (1736 cm^{-1} in MeOH, 1741 cm^{-1} in $CHCl_3$), calibrated by IR spectra of standard solutions of methyl acetate in the CIR cell under the conditions of the catalytic reaction, to give an effective extinction coefficient, $\varepsilon_{eff\,(1736)} = 6.52\ mol^{-1}$ (MeOH). Example calculation (100 mg catalyst **3** containing 4.4×10^{-5} mol Rh, 0.8 M MeI in MeOH (total volume 10 cm^3), 120 °C, 10 bar CO):

Slope Abs(1736 cm^{-1}) vs time = 0.0114 h^{-1}

d(*n*MeOAc)/dt = 0.0114 h^{-1}/6.52 mol^{-1} = 1.75×10^{-3} mol h^{-1}

TOF = 1.75×10^{-3} mol h^{-1} / 4.4×10^{-5} mol = 39.7 h^{-1}

Experiments using $CHCl_3$ solvent

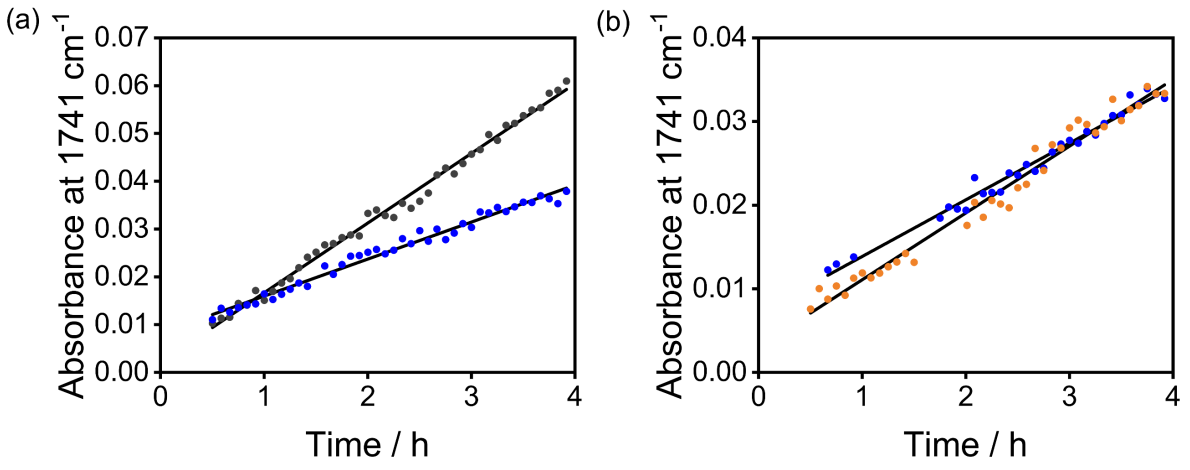

Figure S11. (a) Plots of absorbance *vs*. time for ν(C=O) of MeOAc during carbonylation experiments using **3** (blue) or $Bu_4N[Rh(CO)_2I_2]$ (grey) (120 °C, 10 bar CO, 0.8 M MeI, 2.5 M MeOH in $CHCl_3$; (b) comparison of absorbance *vs*. time plots for initial run (blue) and a subsequent experiment using the recovered catalyst (orange) illustrating retention of activity.

References

1. A. B. Pangborn, M. A. Giardello, R. H. Grubbs, R. K. Rosen and F. J. Timmers, *Organometallics*, 1996, **15**, 1518-1520.
2. J. A. McCleverty, G. Wilkinson, L. G. Lipson, M. L. Maddox and H. D. Kaesz, *Inorg. Synth.*, 1966, **8**, 211-214.
3. A. Fulford, C. E. Hickey and P. M. Maitlis, *J. Organomet. Chem.*, 1990, **398**, 311-323.
4. J. S. Trent, *Macromolecules*, 1984, **17**, 2930-2931.
5. B. R. Pauw, A. J. Smith, T. Snow, N. J. Terrill and A. F. Thünemann, *J. Appl. Crystallogr.*, 2017, **50**, 1800-1811.
6. J. Ilavsky and P. R. Jemian, *J. Appl. Crystallogr.*, 2009, **42**, 347-353.